Supplementary Material

PET/CT imaging

All subjects were studied in the early morning after ≥6 h fasting. Serum glucose was assessed, and an antecubital vein was cannulated. According to current guidelines (1), patients were invited to lye for 20 min in a silent and darkened room, with eyes closed and ears unplugged. A bolus of FDG (4.8 5.2 MBq/kg body weight) was then injected 45-60 minutes before 3D-scan using an integrated PET/CT scanner (Hirez 16, Siemens Medical Solutions or Discovery GE Healthcare). In all cases, the 15 minutes cerebral acquisition was followed by whole body imaging in arms down position.

In both centers, PET data were reconstructed into a 128 × 128 matrix using a 3D iterative reconstruction algorithm (three iterative steps, eight subsets). Raw images were scatter-corrected and processed using a 3D Gaussian filter, while CT was used for attenuation correction.

Image quality control documented a spatial resolution of 4.0 mm full-width at half-maximum for both scanners. According to standard procedures of both labs, the two imaging systems were cross calibrated using a cylinder of 20 cm diameter and 20 cm length filled with a solution containing 100 MBq of ^{68}Ge. Images were reconstructed with the same algorithm used for the clinical protocol.

Hough Transform utilization

Image analysis was performed by means of a pattern recognition algorithm based on an extension of the Hough transform to algebraic curve. The computational method has been previously described (3). Briefly for the current study, we first observed that SC profile is reliably approximated by an ellipse. Let $p = (x_p, y_p)$ be a point in the image plane satisfying the equation of the ellipse

$$\mathcal{C}_{a,b}: \frac{x^2}{a^2} + \frac{y^2}{b^2} = 1 \ .$$

Then, the Hough transform of p with respect to the family of curves $\mathcal{F} = \{\mathcal{C}_{a,b}\}$, is the curve $\Gamma_p(\mathcal{F})$ of equation

$$\Gamma_p(\mathcal{F}): B^2 x_p^2 + A^2 y_p^2 = A^2 B^2$$

in the parameter space $\langle A, B \rangle$ where the two real, positive, and independent parameters a, b vary. The Hough transform method relies on the mathematical fact that when p varies on $\mathcal{C}_{a,b}$, then all curves $\Gamma_p(\mathcal{F})$ intersect in exactly one point in the parameter space. From a computational viewpoint this fact naturally inspires a pattern recognition method according to which the parameter space is discretized in cells, an accumulator function is defined on it, and the ellipse in the image space is identified by the parameters providing the maximum of such function. We first point out that this method can be extended to the recognition of a vast class of algebraic curves in the image space. Second, Beltrametti et al (3) showed that the method is robust with respect to both image noise and spatial inaccuracy in the image. Finally, the Hough transform technique shows a better sensitivity with respect to standard gradient-based methods, since it behaves reliably even in the case of low contrast.

Brain PET preprocessing and statistical analysis in SPM

Original DICOM images were converted to NifTI-1 format using SPM8 DICOM Import (4). PET images were normalized to a customized previously published template (5) and smoothed with 8-mm full width at half maximum Gaussian Kernel. Subsequently, tracer distribution was scaled for whole brain radioactivity concentration to identify areas of relative hypo- or hypermetabolism in ALS group by means of a two-sample *t* test. The same algorithm was used to analyze FDG distribution within ALS group according to either disease presentation (bulbar or spinal) or side involvement at diagnosis. Finally, multiple regression analysis was performed to identify areas whose metabolism was directly o inversely correlated with SC SUV. This analysis was performed without any a priori definition, considering SC SUV as covariate. Age, gender and center of belonging were included as nuisance in all SPM analyses with significance threshold set at $p<0.05$, False-Discovery-Rate (FDR)-corrected both at peak and at cluster level. Only significant clusters

containing at least 100 voxels were taken into consideration. Brain Map Ginger ALE 2.3 (Eickhoff SB, Laird AR.) was used to convert coordinates of significant clusters in Montreal Neurological Institute space into Talairach coordinates. Brodmann areas (BAs) were then identified at a range of 0 to 3 mm from the corrected Talairach coordinates of the SPM output isocenters, after importing the corrected coordinates by means of Talairach client (http://www.talairach.org/index.html).

Supplementary Table 1: Demographic characteristics of patient's population.

Number	44
Age (years)	64±10
Men	25
Women	19
Spinal onset	35 (80%)
Bulbar onset	9 (20%)
Right sided	16/35
Left sided	14/35
Bilateral	5/35
Upper limb onset	12 / 35
Lower limb onset	21 / 35
Combined limbs onset	2 / 35
Time elapsed from ALS diagnosis and PET/CT imaging (months)	10±9
ALS functional rating scale	39±5

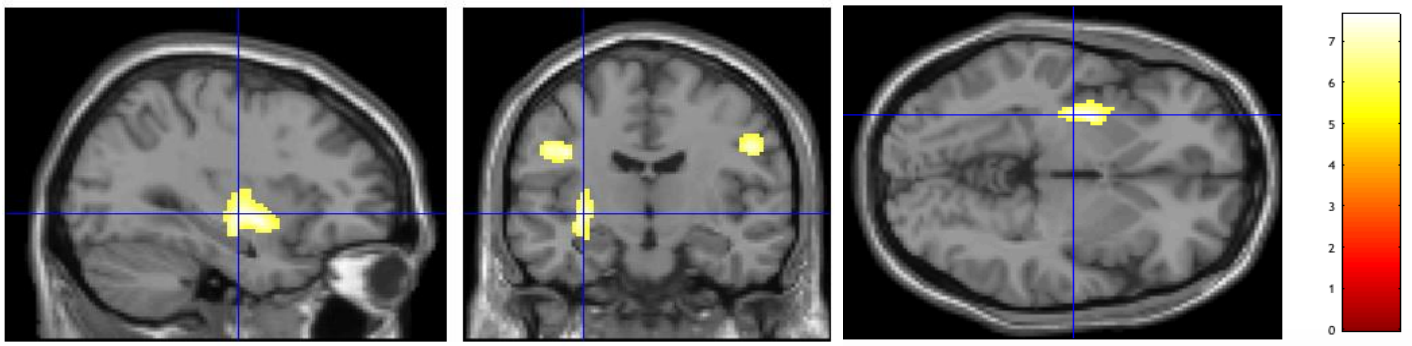

Supplementary Figure 1: Clusters of relative hypometabolism in bulbar vs spinal ALS.

	Cluster Level		**Peak Level**					
Cluster Extent	corrected P value	Cortical region	Maximum Z score	Talairach Coordinates			Cortical Region	BA
547	0.0001	L-Sub Lobar	5.75	-29	-4	-1	Putamen	
		L-Sub Lobar	5.57	-31	-12	0	Putamen	
		L-Frontal	5.25	-22	6	-11	Subcallosal Gyrus	34
		L-Frontal	5.66	-37	-13	29	Precentral Gyrus	6
131	0.0001	R-Frontal	5.53	50	-9	31	Precentral Gyrus	6
131	0.0001	R-Frontal	4.98	41	-12	40	Precentral Gyrus	6

Supplementary Figure 1: Topographic localization of hypometabolic clusters in bulbar vs spinal ALS. Cluster were regarded as significant if they survived at $p<0.05$, FWE corrected at $p<0.05$, FWE corrected. Cluster extension and localization are also described in the table reported below the figure. Bulbar phenotype was characterized by a more pronounced metabolic impairment in bilateral pre-central gyri and in left Putamen. This finding agrees with data by Kim et al. (6) who reported that the putamen was among the most atrophic brain regions in ALS patients. On the other hand, the finding of a relatively reduced bilateral frontal metabolism supports the growing evidence of extramotor changes in bulbar pathology (7) and seems to confirm the divergent neuropsychological and functional patterns in bulbar and spinal onset ALS.

Supplementary Figure 2: Comparison between right and left ALS clinical onset.

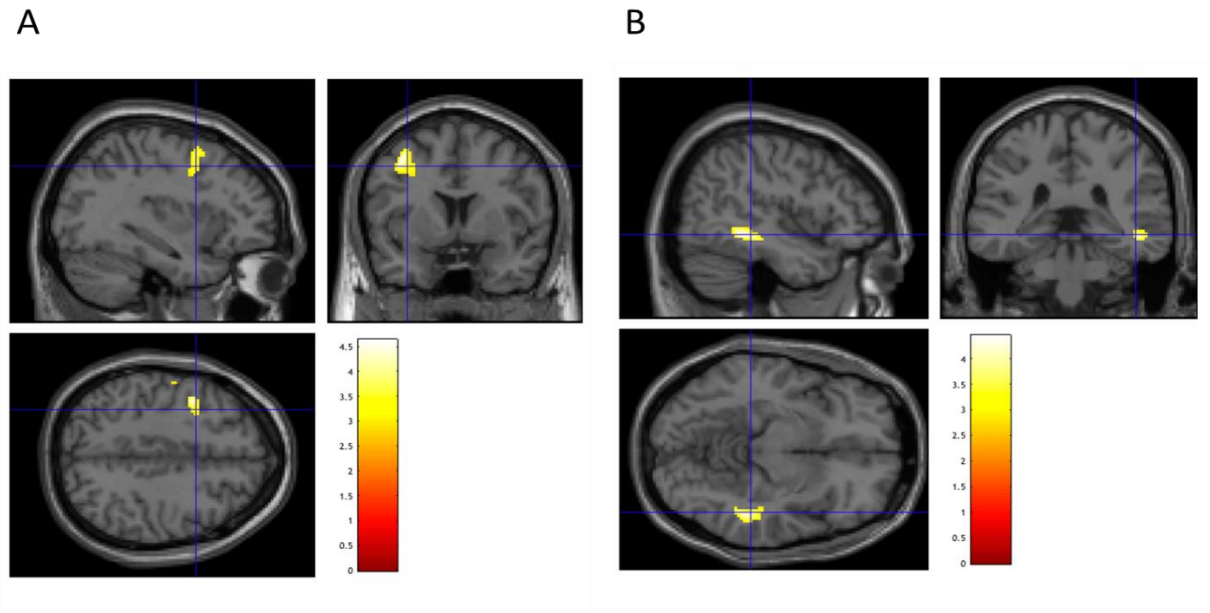

LEFT < RIGHT

	Cluster Level		**Peak Level**					
Cluster Extent	corrected P value	Cortical region	Maximum Z score	Talairach Coordinates			Cortical Region	BA
286	0.022	L-Temporal	3.77	-49	-63	11	Middle Temporal Gyrus	39
		L-Temporal	3.57	-56	-68	25	Middle Temporal Gyrus	39
225	0.038	L-Limbic	3.70	-19	-57	6	Posterior Cingulate	30
204	0.047	R-Frontal	3.69	32	-25	65	Precentral Gyrus	4
		R-Parietal	3.15	45	-25	60	Postcentral Gyrus	3
		R-Parietal	3.00	41	-31	46	Inferior Parietal Lobule	40
173	0.064	L-Frontal	3.68	-37	7	44	Middle Frontal Gyrus	6
145	0.087	L-Frontal	3.37	-54	-7	34	Precentral Gyrus	6
		L-Frontal	2.85	-43	-11	31	Precentral Gyrus	6

RIGHT < LEFT

	Cluster Level		**Peak Level**					
Cluster Extent	corrected P value	Cortical region	Maximum Z score	Talairach Coordinates			Cortical Region	BA
154	0.079	R-Temporal	3.66	44	-44	-2	Sub-Gyral	37

Supplementary Figure 2: Comparison between right and left ALS clinical onset. Cluster were regarded as significant if they survived at $p<0.005$, no FWE corrected. SPM analysis was performed with threshold set at $p<0.005$ no FWE corrected. Panel A shows the topographic representation of clusters in which FDG uptake was significantly lower in right than in left clinical onset ALS patients. Panel B represents the clusters in which FDG uptake was significantly lower in left than in right clinical onset ALS patients. Cluster extension and localization are also described in the corresponding tables. Right onset ALS was associated with a more severe metabolic impairment in the left hemisphere at SPM analysis. However, this finding has to be cautiously interpreted due to the possible occurrence of several biases related to the limited sample size and the variable side with most prominent symptoms at time of scan.

References of the Supplementary Material

(1) Varrone A, Asenbaum S, Vander Borght T, Booij J, Nobili F, Någren K, *et al*. EANM procedure guidelines for PET brain imaging using [18F]FDG, version 2. Eur J Nucl Med Mol Imaging. 2009;36(12):2103-10.

(2) Ricca G, Beltrametti M C, Massone A M. Detecting curves of symmetry in image via Hough transform. Math Comp Sci. 2016;10(1):179-205.

(3) Beltrametti MC, Massone AM, Piana M. Hough transform of special classes of curves. SIAM J Imaging Sci. 2013;6:391-412.

(4) Friston KJ, Frith CD, Liddle PF, Frackowiak RS. Functional connectivity: the principal-component analysis of large (PET) data sets. J Cereb Blood Flow Metab. 1993;13:5-14..

(5) Morbelli S, Rodriguez G, Mignone A, Altrinetti V, Brugnolo A, Piccardo A, *et al*. The need of appropriate brain SPECT templates for SPM comparisons. Q J Nucl Med Mol Imaging. 2008;52:89-98.

(6) Kim HJ, Oh SI, de Leon M, Wang X, Oh KW, Park JS, *et al*. Structural explanation of poor prognosis of amyotrophic lateral sclerosis in the nondemented state. Eur J Neurol. 2016;24:122-9.

(7) Cistaro A, Valentini MC, Chiò A, Nobili F, Calvo A, Moglia C, *et al*. Brain hypermetabolism in amyotrophic lateral sclerosis: a FDG PET study in ALS of spinal and bulbar onset. Eur J Nucl Med Mol Imaging. 2012;39:251-9.